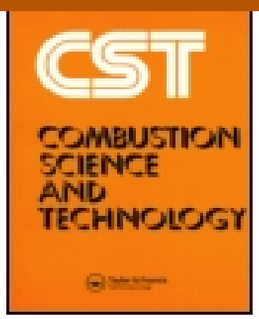

Combustion Science and Technology

ISSN: 0010-2202 (Print) 1563-521X (Online) Journal homepage: http://www.tandfonline.com/loi/gcst20

Effects of oxygenate additives on polycyclic aromatic hydrocarbons(pahs) and soot formation

Fikret Inal & Selim M. Senkan

To cite this article: Fikret Inal & Selim M. Senkan (2002) Effects of oxygenate additives on polycyclic aromatic hydrocarbons(pahs) and soot formation, Combustion Science and Technology, 174:9, 1-19, DOI: 10.1080/00102200290021353

To link to this article: http://dx.doi.org/10.1080/00102200290021353

Published online: 17 Sep 2010.

Combust. Sci. and Tech., 174(9): 1–19, 2002

0010-2202/02 $12.00 + .00
DOI: 10.1080/00102200290021353

EFFECTS OF OXYGENATE ADDITIVES ON POLYCYCLIC AROMATIC HYDROCARBONS (PAHs) AND SOOT FORMATION

FIKRET INAL*

Department of Chemical Engineering,
Izmir Institute of Technology, Urla-Izmir, Turkey

SELIM M. SENKAN

Department of Chemical Engineering,
University of California Los Angeles,
Los Angeles, California, USA

Effects of three oxygenate additives (methanol, ethanol, and MTBE) on the formation of polycyclic aromatic hydrocarbons (PAHs) and soot in laminar, premixed, atmospheric pressure, fuel-rich flames of *n*-heptane were studied at an equivalence ratio of 2.10. A heated quartz microprobe coupled to online gas chromatography/mass spectrometry was used to establish the identities and absolute concentrations of major, minor, and trace species by the direct analysis of samples withdrawn from the flames. Benzene was the most abundant aromatic compound identified. The largest PAH detected was the family of $C_{18}H_{10}$ (molecular weight of 226) that includes cyclopenta[cd]pyrene and benzo[ghi]fluoranthene. Soot particle diameters, number densities, and volume fractions were determined using classical light scattering and extinction measurements. All the oxygenate additives studied reduced the mole fractions of aromatic and PAH species, as well as soot formation. However, the reduction in soot formation was comparable for different oxygenates under the experimental conditions investigated.

Received 14 August 2001; accepted 23 May 2002.

This research was supported in part by the National Science Foundation, the U.S. Environmental Protection Agency, and the UCLA Center for Clean Technologies.

*Address correspondence to inal@likya.iyte.edu.tr

Keywords: PAH, soot, oxygenate additives, premixed flames, hydrocarbon combustion

INTRODUCTION

Fuel oxygenates were first used as an octane replacement for lead in gasoline and later were recognized for their ability to reduce exhaust CO emissions from motor vehicles by leaning the fuel–air mixture. Because CO pollution is predominantly caused by incomplete combustion of motor vehicle fuels, the Clean Air Act Amendments of 1990 required the use of oxygenated gasoline in areas that are in noncompliance with the National Ambient Air Quality Standard for CO. Oxygenates are also low in atmospheric reactivity. Initially, the focus for oxygenates was on several ethers (methyl tertiary-butyl ether [MTBE], ethyl tertiary-butyl ether [ETBE], tertiary amyl methyl ether [TAME]) and alcohols (methanol, ethanol, and tertiary butyl alcohol [TBA]). MTBE and ethanol are the most common oxygenate additives currently used in gasoline. However, the U.S. EPA recently decided to request Congress to phase out use of MTBE as an oxygenate, primarily because of the increase in number of groundwater contamination problems since the oxygenated fuel program started.

n-Heptane is a component of commercial gasoline and is also one of the primary reference fuels for the determination of octane number. The oxidation and pyrolysis of *n*-heptane were investigated in shock tubes (Burcat, 1981; Ciezki and Adomeit, 1987), jet-stirred reactors (Chakir et al., 1992; Dagaut et al., 1995), premixed (Bakali et al., 1998; Doute et al., 1997; Ingemarsson et al., 1999; Westmoreland et al., 1980) and diffusion (Hamins and Seshadri, 1987; Peterca and Marconi, 1989) flames.

Westmoreland et al. (1980) studied PAH and soot formation in a premixed flame of *n*-heptane at an equivalence ratio of 2.05. Postflame samples were taken using glass filter and XAD-2 polymeric resin adsorbent. The most abundant PAH compound was acenaphthylene. Neither the PAH nor major species concentration profiles as a function of distance from the burner were reported. Doute et al. (1997) obtained the mole fraction profiles of stable species and free radicals in low-pressure (6.0 kPa), premixed, laminar *n*-heptane/oxygen/Ar flames using molecular beam mass spectrometry. In subsequent studies, premixed flat flames of *n*-heptane at atmospheric pressure were investigated using unheated microprobe sampling and gas chromatography/mass spectrometry

(GC/MS) both by Bakali et al. (1998) and Ingemarsson et al. (1999) at equivalence ratios of 1.9 and 1.0, respectively. Consequently, only the lower molecular weight (e.g., up to benzene) species concentration profiles were reported by these investigators.

PAHs in laminar diffusion flames of *n*-heptane were reported by Peterca and Marconi (1989) based on the analysis of the fluorescence spectra. Species reported were naphthalene, acenaphthylene, phenanthrene, anthracene, pyrene, fluoranthene, perylene, 3,4-benzopyrene, anthanthrene, coronene, and 1,12-benzoperylene. Acenaphthylene and naphthalene were the most abundant PAHs, a result that is in agreement with premixed flame measurements (Westmoreland et al., 1980). The maximum soot volume fraction reported was $f_v = 3.3 \times 10^{-7}$.

Effects of additives on ignition delay time of *n*-heptane were studied by Levinson (1965) in shock tube experiments. The additives studied were ethylene, 1-butene, toluene, methane, tetraethyl lead, ethane, 2-iodopropane, di-*t*-butylperoxide, acetaldehyde, carbon monoxide, and hydrogen. In the absence of additives the observed ignition delays for lean and slightly rich mixtures were proportional to the ratio of heptane to oxygen in the pressure range 760 to 1370 mmHg. The ignition delays were lengthened by addition of a number of hydrocarbons including increased heptane concentration. Ethane and acetylene were exceptions.

The oxidation of *n*-heptane in the presence of MTBE (*n*-heptane–MTBE 50:50) and ETBE (*n*-heptane–ETBE 50:50) was studied by Dagaut et al. (1997) in a high-pressure jet-stirred reactor ($T = 570$–1170 K, $P = 10$ atm, and $\phi = 1$). Concentration profiles of O_2, CO, CO_2, *n*-C_7H_{16}, CH_4, C_2H_4, MTBE, ETBE, HCHO, CH_3CHO, C_3H_6, 1,3-C_4H_6, and i-C_4H_8 were reported as a function of temperature.

In this study, we report the effects of oxygenates on PAHs and soot formation in premixed *n*-heptane/oxygenate flames at an equivalence ratio of 2.10 (C/O = 0.67) using methanol, ethanol, and MTBE as oxygenate additives.

EXPERIMENTAL

An illustration of the experimental system used is shown in Figure 1. Laminar premixed flat flames of *n*-$C_7H_{16}/O_2/Ar$ and *n*-C_7H_{16}/oxygenate/O_2/Ar at atmospheric pressure were stabilized over a 50-mm-diameter porous bronze burner. Ar was also used as a shield gas to protect the

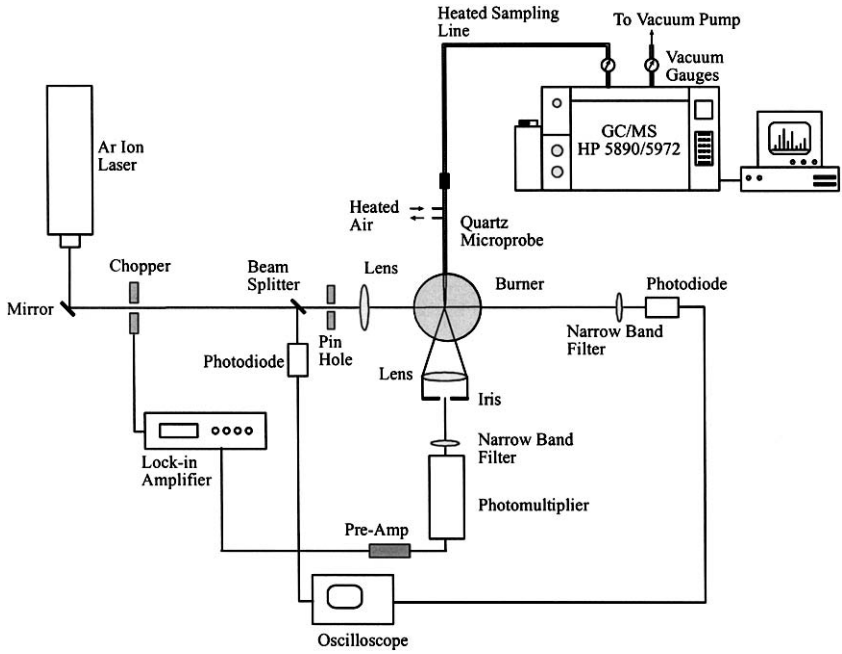

Figure 1. Experimental setup.

flames from surrounding air. Oxygen (99.99%) and argon (99%) were obtained from Airco Welding Supply (Pomona, CA). Liquid fuel and oxygenates were acquired from the following vendors: *n*-heptane (99%) and MTBE (HPLC grade) from Sigma Aldrich, methanol (99.9%) from Fisher Scientific, and ethanol (HPLC grade) from Spectrum Quality Products. The flow rates of oxygen and argon were controlled by calibrated mass flow controllers (Model 247C, MKS). Two high-precision syringe pumps (Isco model 260D with Series D pump controller) were used to introduce the fuel and oxygenate into preheated mixtures of argon–oxygen stream at 150°C. The syringe pumps had flow-rate resolution of 1 μl/min and flow rate accuracy of ±0.5%. The argon shield gas was also heated to the temperature of reactant mixture to prevent condensation. Temperatures at different locations of the fuel delivery system were monitored and kept constant by a multichannel temperature readout and proportional temperature controllers (Omega Engineering Inc.).

The flame samples were withdrawn with an air-heated quartz microprobe at a temperature of about 300°C (Figure 1). Samples were then transferred through a heated, glass-lined stainless steel sampling line to a GC/MS system (HP 5890 Series II/5972) for analysis. A computer-controlled air-actuated multiport solenoid valve system was used to achieve simultaneous injection of samples to capillary (HP–5, 60 m × 0.25 mm × 0.25 μm) and packed bed columns (6-ft Hayesep T and 30-ft Hayesep DB, Alltech). The packed bed columns were connected to a thermal conductivity detector (TCD) for the analysis of low-molecular-weight species. The capillary column was used for higher molecular weight species and connected to a quadruple mass spectrometer.

The GC oven temperature was set to 0°C initially and was held there for 3.45 min. The oven temperature was then increased at a rate of 15°C/min to 160°C and held at that level for 3.33 min. The Hayesep T column was removed from the oven and the temperature was ramped again at 35°C/min until it reached 300°C where it stayed for 10 min.

Species quantifications were done either directly using calibration standards (Matheson Gas, Sigma Aldrich) or by the use of the ionization cross-section method (Fitch and Sauter, 1983). The accuracy of the latter method was reported to be within a factor of two (Castaldi et al., 1995). We estimated an accuracy of about ±15% for the mole fractions of species determined by direct calibration.

To minimize the thermocouple exposure to soot, the flame temperatures were measured using the rapid insertion technique. In this approach, a clean (soot-free), silicon oxide-coated Pt-13% Rh/Pt, 0.075 mm thermocouple was rapidly inserted into the flame using a stepper-motor-driven system (nuDrive, National Instruments). The motion control and data acquisition (5508Sci, American Data Acquisition Corporation) functions were synchronized by a personal computer using LabVIEW (National Instruments). After each measurement, the thermocouple was withdrawn from the flame and the accumulated soot was burnt off using a small propane torch. The temperature profiles reported in this study correspond to direct thermocouple readings and were not corrected for radiation losses.

Soot-particle diameters, number densities, and volume fractions were determined using classical laser light scattering and extinction measurements (Flower, 1986; Figure 1). The light source used was an argon ion laser (Spectra Physics, 2037) with 514.5-nm line at a power of 1 W. A photomultiplier tube (PMT; Hamamatsu, R1463) was used to measure

the relative intensity of the fraction of the incident light scattered at 90° by the soot particles. The transmitted light was measured with a photodiode (Hamamatsu, 51336-BQ) and recorded with an oscilloscope. To obtain high signal-to-noise ratio, it was necessary to minimize the light from all other sources, e.g., flame luminosity and ambient light. Two devices were used to achieve this objective: (1) narrow band-pass filters were placed in front of the PMT and photodiode and (2) the laser light was chopped at a frequency of 1000 Hz and the PMT signals were read using a lock-in amplifier (EG&G 5205).

The experimental setup was calibrated with a known particle-free gas flow composed of only argon. Soot particle size, number density, and volume fraction calculations were carried out by assuming monodisperse particles having a complex refractive index of $1.54–0.58i$ (Faeth and Koylu, 1995; Flower, 1986).

RESULTS AND DISCUSSION

The pre-reaction compositions of the reactant mixtures studied are shown in Table 1. A number of issues regarding the selection of these conditions should be noted. To better compare the effects of oxygenate additives on flame structure and pollutant formation, all the flames were studied under similar conditions. First, all the flames were maintained at the same equivalence ratio of 2.10. This equivalence ratio was determined by trial and error to provide a stable sooting flame that can be studied using our standard sampling microprobes (Castaldi et al., 1995). Higher equivalence ratios resulted in excessive soot formation, which in return plugged the sampling probe orifice, thereby necessitating the early termination of the experiments. At lower equivalence ratios, the flames did not produce as much PAH. Second, the argon dilution was kept at about 66% in all flames. Lower argon dilution led to excess soot formation, and higher dilutions led to weakly stabilized flames that were difficult to probe. Finally, the oxygen weight percent in the *n*-heptane/oxygenate mixtures was kept at 2.7 for each oxygenate studied.

The temperature profiles for the *n*-heptane and *n*-heptane/oxygenate flames are presented in Figure 2. In this and subsequent figures, lines have been drawn through the data points (indicated by symbols) to illustrate trends. As can be seen from this figure, the peak temperatures of all the oxygenate-containing flames were slightly higher than the *n*-heptane

Table 1. The precombustion compositions of the flames studied at equivalence ratio of 2.10

Flame	Mole %
n-Heptane flame	
n-Heptane	5.50
O_2	28.79
Ar	65.71
n-Heptane + MTBE flame	
n-Heptane	4.70
MTBE	1.02
O_2	28.28
Ar	66.00
n-Heptane + methanol flame	
n-Heptane	5.20
Methanol	1.07
O_2	28.03
Ar	65.70
n-Heptane + ethanol flame	
n-Heptane	5.07
Ethanol	1.08
O_2	28.07
Ar	65.78

flame. The peak temperature was 1528 K for the *n*-heptane flame, while these levels were 1550, 1565, and 1571 K for the flames containing methanol, MTBE, and ethanol, respectively. Bakali et al. (1998) reported a maximum flame temperature of about 1600 K in their premixed *n*-heptane flame at an equivalence ratio of 1.9, which is slightly higher than our temperature measurement because their flame was leaner.

In Figures 3 and 4, the mole fraction profiles of CO, acetylene (C_2H_2), 1,2 propadiene/1-propyne (C_3H_4), diacetylene (C_4H_2), and vinylacetylene (C_4H_4) are presented for all the flames studied. As can be seen from these figures, the mole fraction profiles of these low-molecular-weight reaction products were consistently lower in flames containing the oxygenates. C_2H_2 and C_4H_2 were the primary hydrocarbon species detected with maximum mole fractions of 4.7×10^{-2} and 9.3×10^{-3}, respectively, in the *n*-heptane flame. Their peak mole fractions were in the postflame region for all the flames studied. With the exception of C_4H_2, the mole fractions of these low-molecular-weight hydrocarbon species (i.e., C_2H_2,

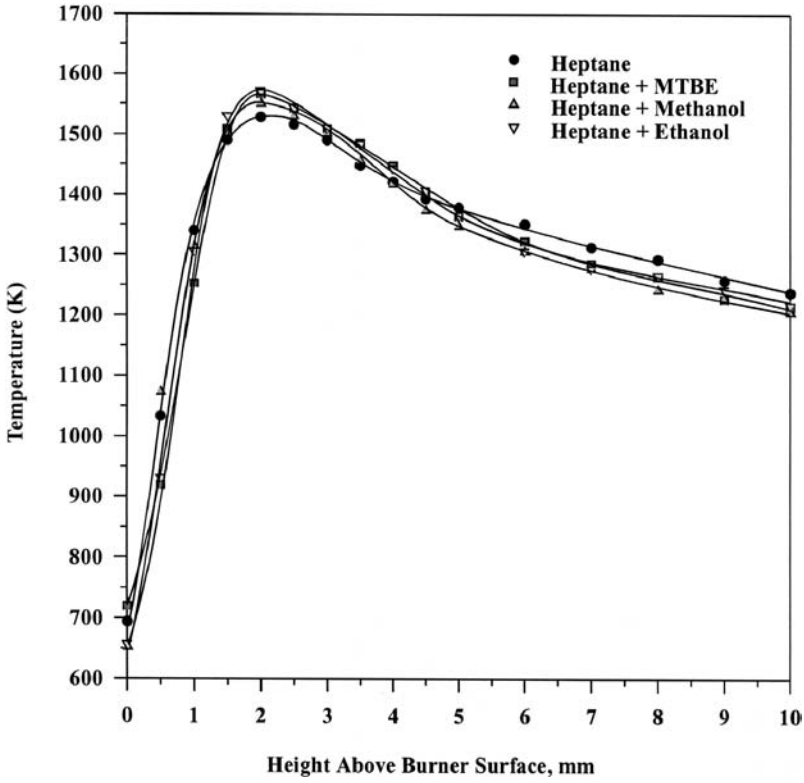

Figure 2. Flame temperatures.

C_3H_4, and C_4H_4) in *n*-heptane flame are similar to those reported earlier for the premixed combustion of *n*-heptane at fuel-rich condition (Bakali et al., 1998). The reason for the difference in concentrations of C_4H_2 is not clear but it may be attributed to the different reference species used for the calculation of the ionization cross section. However, the mole fraction levels of C_4H_2 reported in this study are of the same order of magnitude as those reported earlier for the fuel-rich, premixed combustion of other hydrocarbon fuels (Marinov et al., 1998; Melton et al., 1998, 2000).

It is well established that at high temperatures, *n*-heptane consumption occurs by the thermal decomposition via C–C bond rupture and H-atom abstraction by a number of radical species (Chakir et al., 1992; Coats and Williams, 1979; Held et al., 1997; Lindstedt and Maurice, 1995).

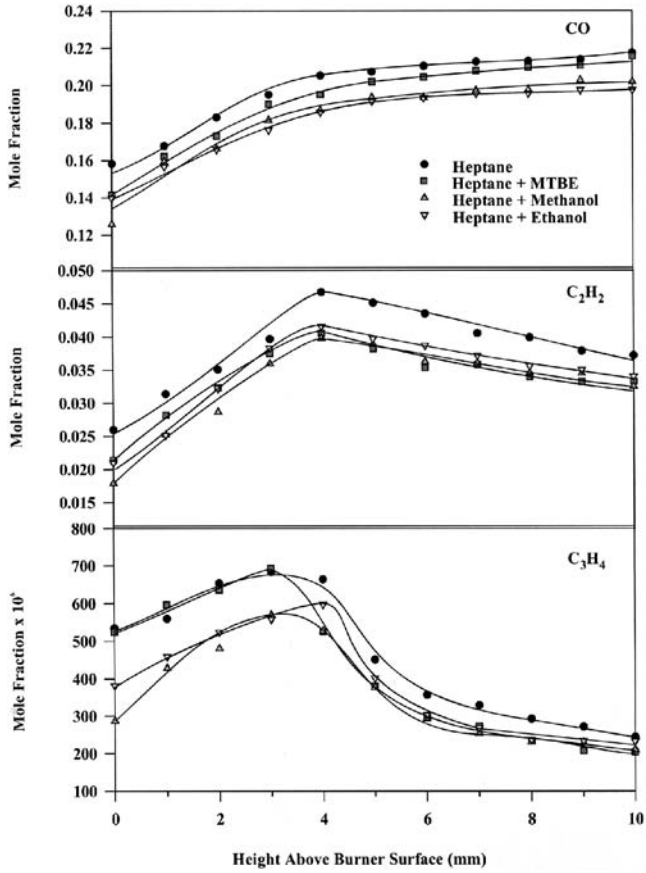

Figure 3. Mole fraction profiles of CO, C_2H_2, and C_3H_4.

$$C_7H_{16} = n\text{-}C_3H_7 + p\text{-}C_4H_9$$

$$C_7H_{16} = 1\text{-}C_5H_{11} + C_2H_5$$

$$C_7H_{16} = 1\text{-}C_6H_{13} + CH_3$$

$$C_7H_{16} + X \rightarrow C_7H_{15} + XH \qquad (X = H, O, OH, HO_2, CH_3)$$

The modeling studies for premixed *n*-heptane flames indicated that the dominant fuel-consumption paths vary as a function of equivalence ratio

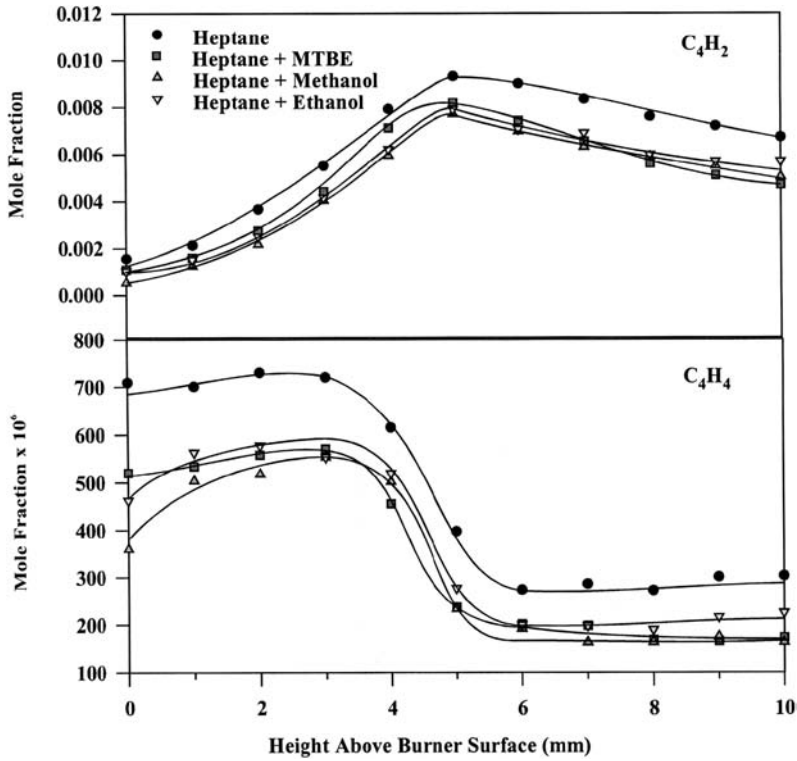

Figure 4. Mole fraction profiles of C_4H_2 and C_4H_4.

and the thermal decomposition path becomes increasingly important at higher equivalence ratios (Held et al., 1997).

The four isomers of *n*-heptyl radical (C_7H_{15}), which are formed by the H-atom abstraction reactions, consume primarily through the β-scission of a C–C bond at high temperatures (Chakir et al., 1992; Dagaut et al., 1994; Held et al., 1997; Lindstedt and Maurice, 1995; Westbrook et al., 1988).

$$1\text{-}C_7H_{15} = C_2H_4 + 1\text{-}C_5H_{11}$$

$$2\text{-}C_7H_{15} = C_3H_6 + p\text{-}C_4H_9$$

$$3\text{-}C_7H_{15} = 1\text{-}C_4H_8 + n\text{-}C_3H_7$$

$$3\text{-}C_7H_{15} = 1\text{-}C_6H_{12} + CH_3$$

$$4\text{-}C_7H_{15} = 1\text{-}C_5H_{10} + C_2H_5$$

In addition to thermal decomposition, isomerization reactions of these four *n*-heptyl radicals are also important.

The initial *n*-heptane concentrations in *n*-heptane/oxygenate fuels were reduced by the addition of oxygenate additives to baseline fuel. The oxygen in additive remains connected to a carbon atom and the carbon atom cannot participate in any of the reactions of small unsaturated species. Therefore, the mole fractions of low-molecular-weight reaction products were reduced by the addition of oxygenates. In addition, the major oxidation pathway of MTBE is unimolecular decomposition producing isobutene and methanol (Dagaut et al., 1997; Norton and Dryer, 1990). Isobutene is less reactive than hydrocarbons formed by the thermal decomposition of *n*-heptane and *n*-heptyl radicals. The production of less-reactive intermediate isobutene also causes a reduction of small hydrocarbons with this additive.

Mole fractions of single-ring aromatics and PAH species were also lower in *n*-heptane/oxygenate flames as shown in Figures 5 to 7. The data obtained within a few millimeters above the burner surface should be considered questionable because of the possible sampling-probe–burner-surface interactions. An examination of these figures indicates that the reduction in some of the aromatic and PAH species concentrations were larger in *n*-heptane/MTBE flames. However, in most cases the differences between the *n*-heptane/MTBE and other *n*-heptane/oxygenate flames were within the accuracy of the experiments. Fluoranthene and pyrene were detected but not quantified in *n*-heptane/methanol flame because of their low levels (Figure 7).

Concentration profiles of most of the aromatic and PAH species peaked at or above 4 mm from the burner surface. Toluene was the exception, which showed an earlier maximum around 1 mm (Figure 5). A similar trend for toluene was also observed for the premixed combustion of other hydrocarbon fuels (Melton et al., 2000).

Benzene was the most abundant aromatic species in all the flames studied with peak mole fractions of 343 ppm in *n*-heptane, 194 ppm in *n*-heptane/MTBE, 211 ppm in *n*-heptane/ethanol, and 194 ppm in *n*-heptane/methanol flames (Figure 5). The maximum benzene mole fraction in *n*-heptane flame was higher by a factor of 4.5 than in that of Bakali et al. (1998).

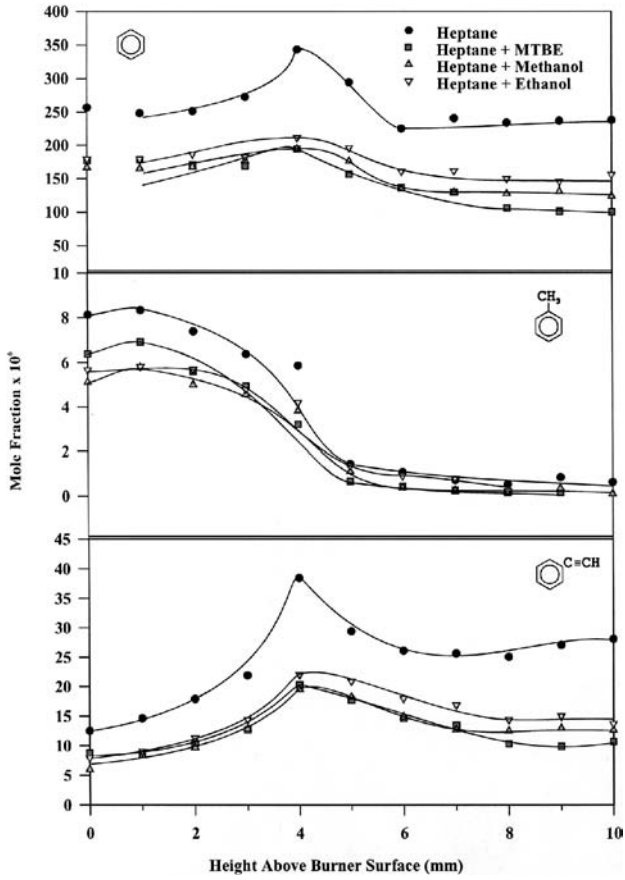

Figure 5. Mole fraction profiles of benzene, toluene, and phenylacetylene.

The reduction in PAH mole fractions is related to the concentrations of small unsaturated hydrocarbons that are known to be responsible for the formation of aromatic and PAH species in flames. Frenklach and Wang (1994) proposed that the formation of the first aromatic ring in flames of nonaromatic fuels usually begins with vinyl addition to acetylene. Vinylacetylene is formed at high temperatures, and followed by acetylene addition to the n-C_4H_3 radical formed by the H abstraction from the vinylacetylene. The benzene can also be formed by the combination of propargyl radicals producing benzene or phenyl (Miller and Melius, 1992). The modeling studies for n-heptane diffusion flames showed that

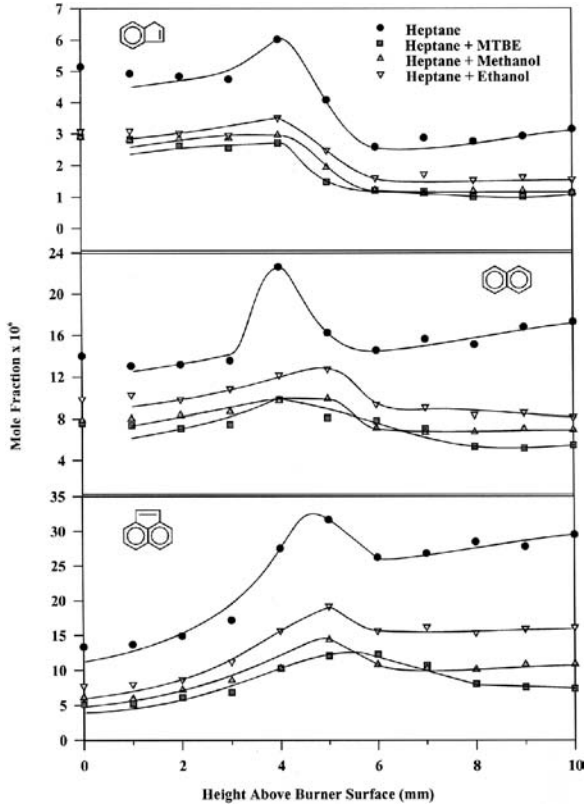

Figure 6. Mole fraction profiles of indene, naphthalene, and acenaphthylene.

benzene formation occurs through both the C_3 and C_4 chains (Lindstedt and Maurice, 1995). The larger aromatics can be built by the addition of nonaromatics such as C_2H_2 and C_4H_5. The addition of aromatic radicals to nonaromatics can also lead to condensed ring compounds (Bittner and Howard, 1981).

Acenaphthylene and naphthalene were the primary PAH compounds in all the flames investigated (Figure 6). The peak mole fractions of acenaphthylene were about 32 ppm in *n*-heptane flame, 12 ppm in *n*-heptane/MTBE flame, 19 ppm in *n*-heptane/ethanol flame, and 10 ppm in *n*-heptane/methanol flame. Similarly, the peak levels of naphthalene were 22 ppm in *n*-heptane and 9.8 ppm, 12 ppm, and 9.7 ppm in MTBE, ethanol, and methanol-containing flames, respectively. Other researchers

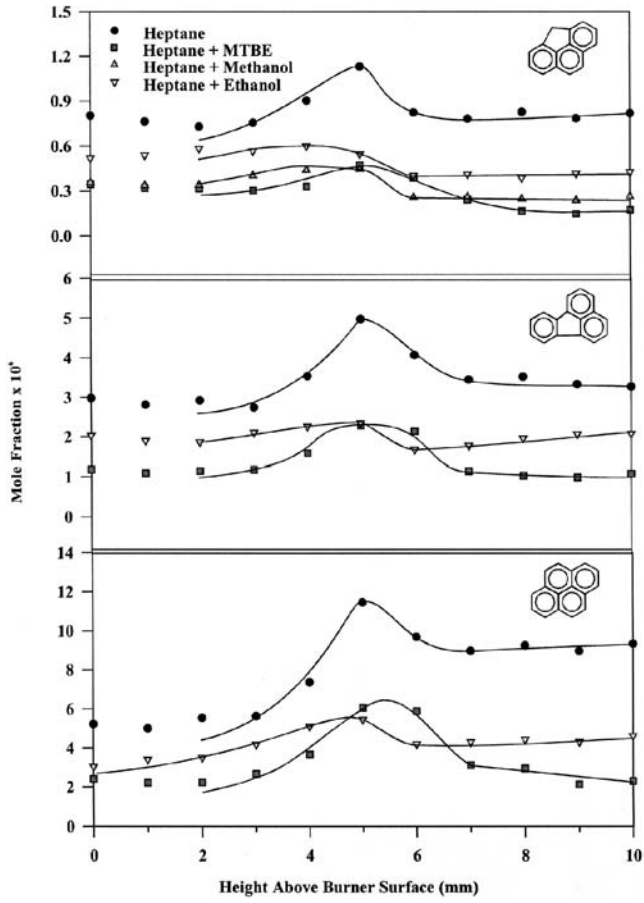

Figure 7. Mole fraction profiles of 4H-cyclopenta[def]phenanthrene, fluoranthene, and pyrene.

also reported acenaphthylene as a major PAH species in premixed and diffusion flames of *n*-heptane (Peterca and Marconi, 1989; Westmoreland et al., 1980).

The largest PAHs detected were the molecular weight (MW) of 226 ($C_{18}H_{10}$) species including cyclopenta[cd]pyrene and benzo[ghi]fluoranthene in the *n*-heptane flame (Figure 8). Their mole fractions were about 8 and 6 ppm, respectively. The concentrations of pyrene (MW 202), and cyclopenta[cd]pyrene (MW 226) were higher than their isomers

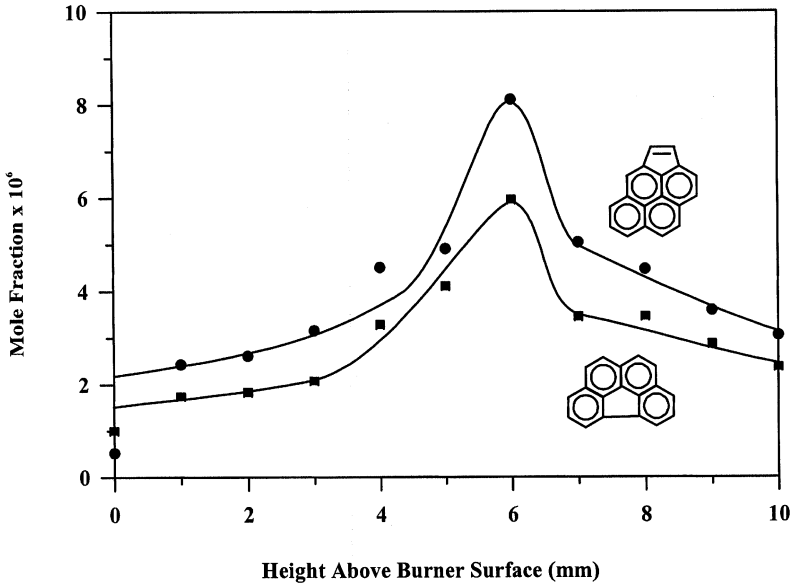

Figure 8. Mole fraction profiles of cyclopenta[cd]pyrene and benzo[ghi]fluoranthene in *n*-heptane flame.

fluoranthene and benzo[ghi]fluoranthene (Figures 7 and 8). However, the difference in isomer concentrations was lower for MW 226 species.

Soot properties were calculated by assuming spherical monodisperse soot particles to comply with Rayleigh scattering approximation. However, nonspherical and polydisperse soot occurs within the flame due to the agglomeration of primary soot particles. The Rayleigh approximation was demonstrated to have a negligible effect on the determination of the soot volume fraction and hold to within a factor of three for the particle diameters (d_p). However, because of d_p^{-3} dependence of particle number density, Rayleigh analysis causes a significant uncertainty in number density estimation (Koylu, 1996). In Figure 9, the soot particle diameters, number densities, and volume fractions are reported for all the flames studied. As seen in this figure, the soot data were acquired only 3 mm above the burner surface due to insignificant soot formation early in the flame zone. The maximum soot particle diameter was about 18 nm and this was observed in the *n*-heptane flame. Soot particle diameters and volume fractions were consistently reduced in all the flames containing

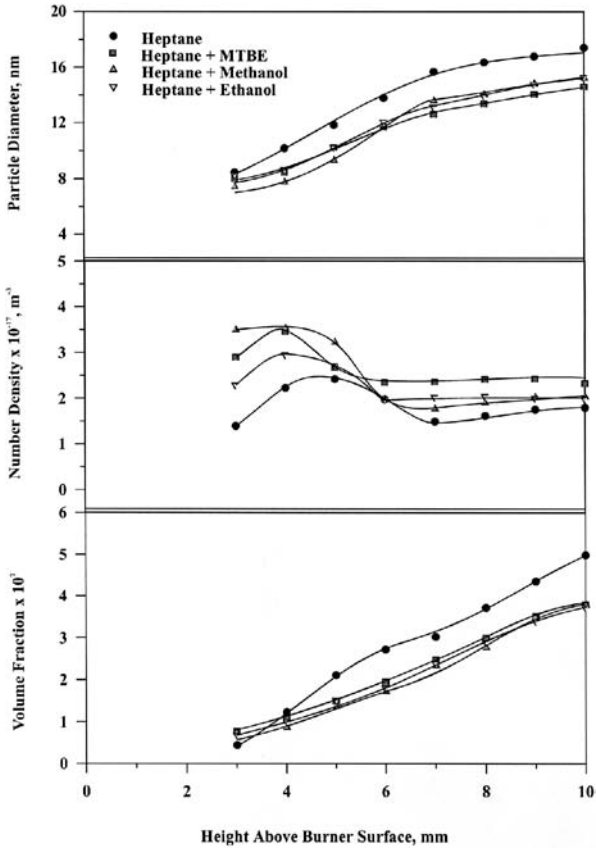

Figure 9. Soot particle diameters, number densities, and volume fractions.

the oxygenates. However, the level of reduction in soot particle diameters and volume fractions were about the same for each oxygenate additive used. Similar results were also obtained in diesel engine studies (Choi and Reitz, 1999).

Several explanations can be offered for the observed particulate reductions by oxygenate additives. First, oxygenate additive modifies the flame chemistry by affecting the soot oxidation reaction rate through an alteration of the concentration of OH radicals. It was suggested that the oxidation of soot in the flame occurs mostly because of the OH radical, because 10% of the collisions of the OH radicals with soot particles results in gasifying of a carbon atom (Haynes, 1991). Second, since

acetylene addition and PAHs are important in soot formation and growth mechanisms (Benish et al., 1996; Frenklach and Wang, 1990; Harris and Weiner, 1983), suppression of soot formation by the decrease in concentrations of these soot precursors may be the reason for the particulate reduction. Third, the temperature affects the two competing processes occurring in premixed sooting flames (Glassman, 1988), i.e., the rate of formation of soot precursors through fuel pyrolysis and the rate of oxidative (OH radical) attack on these precursors. Both rates increase with temperature, but the oxidative attack rate increases faster. Therefore, the higher the temperature, the lesser the tendency of premixed flames to soot.

In conclusion, the presence of oxygenate additives reduced the mole fractions of aromatic and PAH species, as well as soot levels in *n*-heptane flames. However, the extent of reductions was generally similar and did not strongly depend on the structure of the oxygenate additive used because the oxygen concentration was kept at 2.7% wt in *n*-heptane/oxygenate mixtures for each oxygenate investigated.

REFERENCES

Bakali, A.E., Delfau, J.-L., and Vovelle, C. (1998) Experimental study of 1 atmosphere rich, premixed n-heptane and iso-octane flames. *Combust. Sci. Tech.*, **140**, 69–91.

Benish, T.G., Lafeur, A.L., Taghizadeh, K., and Howard, J.B. (1996) C_2H_2 and PAH as soot growth reactants in premixed C_2H_4-Air flames. *Proc. Combust. Instit.*, **26**, 2319–2326.

Bittner, J.D., and Howard, J.B. (1981) Composition profiles and reaction mechanisms in a near-sooting premixed benzene/oxygen/argon flame. *Proc. Combust. Instit.*, **18**, 1105–1116.

Burcat, A. (1981) Shock initiated ignition in heptane-oxygen-argon mixtures. *Int. Symp. on Shock Tubes and Waves*, **13**, 826–833.

Castaldi, M.J., Vincitore, A.M., and Senkan, S.M. (1995) Micro-structures of premixed hydrocarbon flames: Methane. *Combust. Sci. Tech.*, **107**, 1–19.

Chakir, A., Bellimam, M., Boettner, J.C., and Cathonnet, M. (1992) Kinetic study of n-heptane oxidation. *Int. J. Chem. Kinet.*, **24**, 385–410.

Choi, C.Y., and Reitz, R.D. (1999) An experimental study on the effects of oxygenated fuel blends and multiple injection strategies on DI diesel engine emissions. *Fuel*, **78**, 1303–1317.

Ciezki, H., and Adomeit, G. (1987) Experimental shock-tube investigation of the ignition delay of n-heptane-O_2-N_2-Ar mixtures under high pressure. *Int. Symp. on Shock Tubes and Waves*, **16**, 481–486.

Coats, C.M., and Williams, A. (1979) Investigation of the ignition and combustion of n-heptane-oxygen mixtures. *Proc. Combust. Instit.*, **17**, 611–621.

Dagaut, P., Koch, R., and Cathonnet, M. (1997) The oxidation of n-heptane in the presence of oxygenated octane improvers: MTBE and ETBE. *Combust. Sci. Tech.*, **122**, 345–361.

Dagaut, P., Reuillon, M., and Cathonnet, M. (1994) High pressure oxidation of liquid fuels from low to high temperature. 1. n-Heptane and iso-octane. *Combust. Sci. Tech.*, **95**, 233–260.

Dagaut, P., Reuillon, M., and Cathonnet, M. (1995) Experimental study of the oxidation of n-heptane in a jet stirred reactor from low to high temperature and pressures up to 40 atm. *Combust. Flame*, **101**, 132–140.

Doute, C., Delfau, J.L., Akrich, R., and Vovelle, C. (1997) Experimental study of the chemical structure of low-pressure premixed n-heptane-O_2-Ar and iso-octane-O_2-Ar flames. *Combust. Sci. Tech.*, **124**, 249–276.

Faeth, G.M., and Koylu, U.O. (1995) Soot morphology and optical properties in nonpremixed turbulent flame environments. *Combust. Sci. Tech.*, **108**, 207–229.

Fitch, W.L., and Sauter, A.D. (1983) Calculation of relative electron impact total ionization cross sections for organic molecules. *Anal. Chem.*, **55**, 832–835.

Flower, W.L. (1986) Light-scattering measurements of soot particles in flames. *SPIE*, **644**, 28–39.

Frenklach, M., and Wang, H. (1990) Detailed modeling of soot particle nucleation and growth. *Proc. Combust. Instit.*, **23**, 1559–1565.

Frenklach, M., and Wang, H. (1994) Detailed mechanism and modeling of soot particle formation. In H. Bockhorn (Ed.) *Soot Formation in Combustion*, Springer-Verlag, Berlin Heidelberg, Germany, pp. 165–192.

Glassman, I. (1988) Soot formation in combustion processes. *Proc. Combust. Instit.*, **22**, 295–311.

Hamins, A., and Seshadri, K. (1987) The structure of diffusion flames burning pure, binary, and ternary solutions of methanol, heptane, and toluene. *Combust. Flame*, **68**, 295–307.

Harris, S.J., and Weiner, A.M. (1983) Determination of the rate constant for soot surface growth. *Combust. Sci. Tech.*, **32**, 267–275.

Haynes, B.S. (1991) Soot and hydrocarbons in combustion. In W. Bartok, and A.F. Sarofim, (Eds.) *Fossil Fuel Combustion*, Wiley Interscience, New York, pp. 261–327.

Held, T.J., Marchese, A.J., and Dryer, F.L. (1997) A semi-empirical reaction mechanism for n-heptane oxidation and pyrolysis. *Combust. Sci. Tech.*, **123**, 107–146.

Ingemarsson, A.T., Pedersen, J.R., and Olsson, J.O. (1999) Oxidation of n-heptane in a premixed laminar flame. *J. Phys. Chem. A*, **103**, 8222–8230.

Koylu, U.O. (1996) Quantitative analysis of in situ optical diagnotics for inferring particle/aggregate parameters in flames: Implications for soot surface growth and total emissivity. *Combust. Flame*, **109**, 488–500.

Levinson, G.S. (1965) High temperature preflame reactions of n-heptane. *Combust. Flame*, **9**, 63–72.

Lindstedt, R.P., and Maurice, L.Q. (1995) Detailed kinetic modeling of n-heptane combustion. *Combust. Sci. Tech.*, **107**, 317–353.

Marinov, N.M., Pitz, W.J., Westbrook, C.K., Vincitore, A.M., Castaldi, M.J., Senkan, S.M., and Melius, C.F. (1998) Aromatic and polycyclic aromatic hydrocarbon formation in a laminar premixed n-butane flame. *Combust. Flame*, **114**, 192–213.

Melton, T.R., Inal, F., and Senkan, S.M. (2000) The effects of equivalence ratio on the formation of polycyclic aromatic hydrocarbons and soot in premixed ethane flames. *Combust. Flame*, **121**, 671–678.

Melton, T.R., Vincitore, A.M., and Senkan, S.M. (1998) The effects of equivalence ratio on the formation of polycyclic aromatic hydrocarbons and soot in premixed methane flames. *Proc. Combust. Instit.*, **27**, 1631–1637.

Miller, J.A., and Melius, C.F. (1992) Kinetic and thermodynamic issues in the formation of aromatic compounds in flames of aliphatic fuels. *Combust. Flame*, **91**, 21–39.

Norton, T.S., and Dryer, F.L. (1990) The flow reactor oxidation of C_1-C_4 alcohols and MTBE. *Proc. Combust. Instit.*, **23**, 179–185.

Peterca, L., and Marconi, F. (1989) Fluorescence spectra and polycyclic aromatic species in a n-heptane diffusion flame. *Combust. Flame*, **78**, 308–325.

Westbrook, C.K., Warnatz, J., and Pitz, W.J. (1988) A detailed chemical kinetic reaction mechanism for the oxidation of iso-octane and n-heptane over an extended temperature range and its application to analysis of engine knock. *Proc. Combust. Instit.*, **22**, 893–901.

Westmoreland, P.R., Howard, J.B., and Longwell, J.P. (1980) *Second Annual Progress Report—Center for Health Effects of Fossil Fuel Utilization*. MIT.